Synthesis and biological evaluation of Haspin inhibitors: kinase inhibitory potency and cellular activity

Wael Zeinyeh, Yannick Esvan, Béatrice Josselin, Mathilde Defois, Blandine Baratte, Stefan Knapp, Apirat Chaikuad, Fabrice Anizon, Francis Giraud, Sandrine Ruchaud, et al.

▶ **To cite this version:**

Wael Zeinyeh, Yannick Esvan, Béatrice Josselin, Mathilde Defois, Blandine Baratte, et al.. Synthesis and biological evaluation of Haspin inhibitors: kinase inhibitory potency and cellular activity. European Journal of Medicinal Chemistry, 2022, 236, pp.114369. 10.1016/j.ejmech.2022.114369 . hal-03764791

HAL Id: hal-03764791
https://hal.science/hal-03764791v1

Submitted on 30 Aug 2022

HAL is a multi-disciplinary open access archive for the deposit and dissemination of scientific research documents, whether they are published or not. The documents may come from teaching and research institutions in France or abroad, or from public or private research centers.

L'archive ouverte pluridisciplinaire **HAL**, est destinée au dépôt et à la diffusion de documents scientifiques de niveau recherche, publiés ou non, émanant des établissements d'enseignement et de recherche français ou étrangers, des laboratoires publics ou privés.

Synthesis and biological evaluation of Haspin inhibitors: kinase inhibitory potency and cellular activity

Wael Zeinyeh[‡,a], Yannick J. Esvan[‡,a], Béatrice Josselin[†ǂ,a], Mathilde Defois[‡], Blandine Baratte[†ǂ], Stefan Knapp[ǁ,#], Apirat Chaikuad[ǁ,#], Fabrice Anizon[‡], Francis Giraud [‡,*], Sandrine Ruchaud[†,*], Pascale Moreau[‡,*]

[‡] Université Clermont Auvergne, CNRS, Clermont Auvergne INP, ICCF, F-63000 Clermont-Ferrand, France.

[ǁ] Institute of Pharmaceutical Chemistry, Johann Wolfgang Goethe University, Max-von-Laue-Str. 9, 60438, Frankfurt am Main, Germany.

[#] Buchmann Institute for Molecular Life Sciences, Structural Genomics Consortium (SGC), Max-von-Laue-Str. 15, 60438, Frankfurt am Main, Germany.

[†] Sorbonne Université, CNRS, UMR8227, Integrative Biology of Marine Models Laboratory (LBI2M), Station Biologique de Roscoff, 29680 Roscoff, France.

[ǂ] Sorbonne Université, CNRS, FR2424, Plateforme de criblage KISSf (Kinase Inhibitor Specialized Screening facility), Station Biologique de Roscoff, 29680 Roscoff, France;

[a] Authors contributed equally to this work

* Corresponding authors

(PM) Tel: +33 (0) 4 73 40 79 63. E-mail: pascale.moreau@uca.fr

(FG) Tel: +33 (0) 4 73 40 71 27. E-mail: francis.giraud@uca.fr

(SR) Tel: +33 (0) 2 98 29 23 09. E-mail: sandrine.ruchaud@sb-roscoff.fr

Abstract

Haspin (haploid germ cell-specific nuclear protein kinase) offers a potential target for the development of new anticancer drugs. Thus, the identification of new inhibitors targeting this protein kinase is of high interest. However, Haspin inhibitors developed to date show a poor selectivity profile over other protein kinases of the human kinome. Here, we identified a new pyridoquinazoline based inhibitor (**4**), with excellent inhibitory activity and selectivity for Haspin (IC_{50} of 50 nM). We describe the structure-activity relationship study including the evaluation of this inhibitor on a large panel of 486 kinases as well as on immortalized or cancer cell lines. In addition, we determined the binding mode of analogue **2a** in complex with Haspin using X-ray crystallography.

Keywords: pyridoquinazolines; kinase inhibition; Haspin

1. Introduction

As part of our ongoing research dedicated to identification of new anticancer drugs, we focused on new small molecules targeting Haspin (haploid germ cell-specific nuclear protein kinase). Haspin kinase activity is essential during mitosis. Together with Aurora B, Haspin localizes at the centromere and specifically phosphorylates threonine 3 of Histone H3, ensuring proper kinetochore-microtubule attachment as well as maintenance of centromeric cohesion and mitotic spindle. Since Haspin belongs to atypical protein kinase family with an unusual kinase domain architecture, selectivity might be achieved by targeting Haspin unique structural features [1-3]. Due to its role in mitosis regulation, Haspin presents a potential target for the development of new anticancer drugs [4]. This is supported by recent works on cellular repercussions of Haspin inhibition in xenografted nude mice demonstrating its antiangiogenic effects and anticancer potential [5]. On a mechanistic level, Haspin inhibition has been shown to induce cell death as a consequence of mitotic catastrophe, making a compelling case targeting Haspin in cancer [5]. Several Haspin inhibitors (*e.g.* 5-iodotubercidin, CHR-6494, LDN-0192960) have been described [5-9]. These reported kinase inhibitors are ATP-competitive that lack selectivity for Haspin.

More than 500 human protein kinases representing about 2% of the human genome and sharing the same natural substrate (ATP) have been identified [10]. Therefore, the main issue encountered during the development of kinase inhibitors is selectivity. DYRK (dual-specificity tyrosine-(Y)-phosphorylation regulated kinase) and CLK (cdc2-like kinase) are two protein kinase families that are frequently off targets of Haspin inhibitors [11-13]. The reason for this off-target activity is most likely due to a shared bulky residue located N-terminal to the DFG motif that creates a narrow back pocket stabilizing unusual binding modes that anchor inhibitors often to the conserved back pocket lysine glutamate ion pair [14,15].

Recently, we identified a pyrido[3,4-*g*]quinazoline series bearing NO_2 or NH_2 groups at the 10-position as potent inhibitors of DYRK1A and CLK1. Preliminary structure-activity relationship (SAR) results indicated that the introduction of various substituents at different positions of the pyrido[3,4-*g*]quinazoline scaffold can lead to potent nanomolar kinase inhibitors with different selectivity profiles [16-20]. Indeed, we previously demonstrated that the presence of a nitro/amino group at the 10-position is important for the CLK1/DYRK1A inhibition while the introduction of an alkyl/aryl substituent at the 5-position is in favor of CDK5/GSK3 inhibition. Based on frequent DYRK1A/CLK1/Haspin cross-inhibition reported in the literature, this prompted us to study this heteroaromatic structure in more detail aiming at increasing selectivity towards Haspin. Therefore, we focused our synthetic work toward the preparation of derivatives presenting new or diversely substituted heterocycles (Fig. 1).

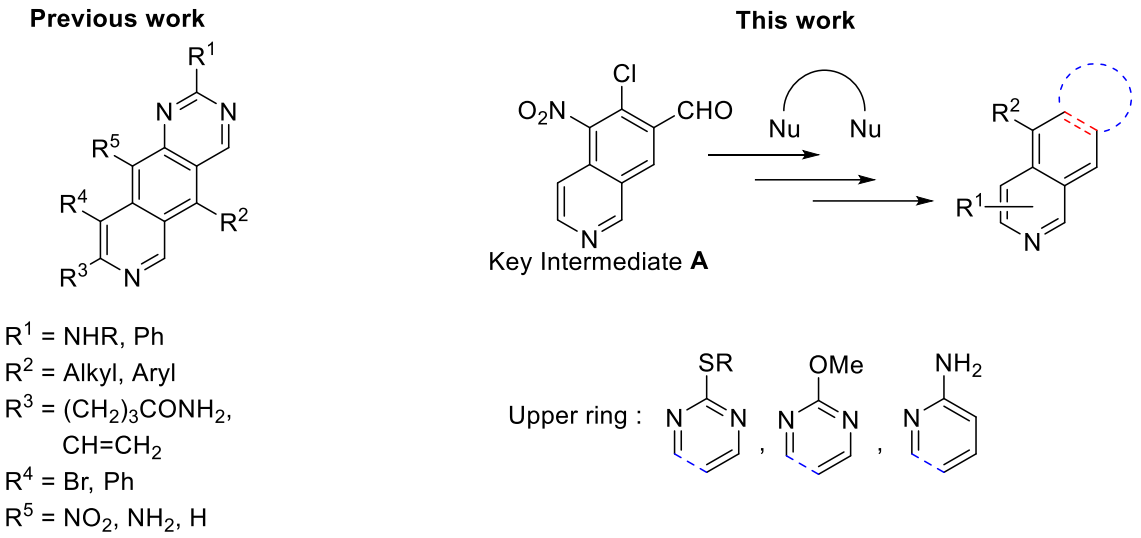

Figure 1. Structural modifications previously applied to the pyridoquinazoline moiety (Previous work) and new ones (This work).

2. Chemistry

2.1. Synthesis of diversely substituted pyridoquinazolines and pyridoquinolines

First of all, using a similar approach as applied in the aminopyrimidine series [16-20], we prepared diversely substituted thio analogues **2a-h** by condensation of *S*-alkylisothiouronium salts and intermediate **A** (Fig. 1). Alkylisothiouronium were either commercially available or easily obtained by alkylation of the corresponding thiourea with various alkyl halide [21] (Scheme 1). These salts were converted in a short time to the desired thiopyrimidines **2a-h** in moderate yields [22]. Is it worth to notice that, in the presence of methylisothiouronium, compound **2a'** was obtained as a side product in 14% yield (Scheme 1). The methylsulfanyl group at the 10-position was introduced by aromatic nucleophilic substitution of the nitro group by a thiomethoxide ion probably formed by decomposition of S-methylisothiouronium in the presence of water.

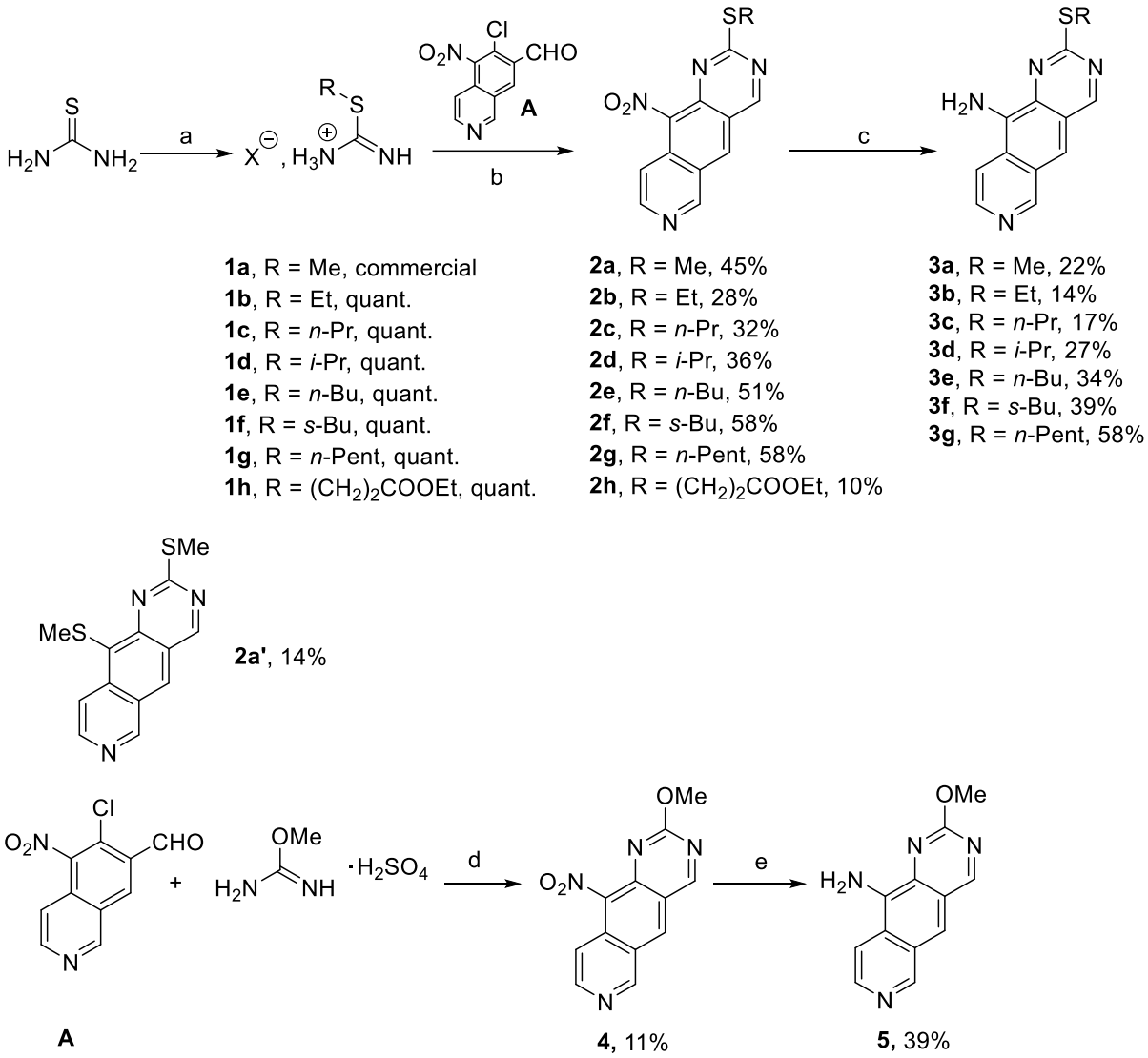

Scheme 1. Synthesis of pyridoquinazolines **2a-h**, **2a'**, **3a-g** and **4, 5**. Reagents and conditions: (a) RX, EtOH (b) $NaHCO_3$, DMA (c) Fe, NH_4Cl, MeOH, H_2O (d) 4 Å Molecular sieves, K_2CO_3, CH_3CN (e) H_2, Pd/C, CH_2Cl_2/MeOH.

Analog **4**, bearing a methoxy group at the 2-position was synthesized similarly using *O*-methylisourea hydrogen sulfate instead of *S*-alkylisothiouronium [23] (Scheme 1). Nitro groups of compounds **2a-g** and **4** were subsequently reduced to the corresponding amino analog **3a-g** and **5** using either iron in the presence of ammonium chloride in MeOH/H_2O or catalytic hydrogenation conditions with Pd/C in CH_2Cl_2/MeOH. Due to purification difficulties, yields ranging from 14% to 58% were observed. Moreover, because of low quantities obtained, we never tried to convert compound **2h** to its amino counterpart.

In order to modify the upper heterocycle, we studied the reactivity between intermediate **A** and acetamidine. This reaction led to pyridoquinoline **6** in 11% yield [23]. However, enough compound was obtained to try the further reduction to the corresponding amino analog **7** (Scheme 2). Unfortunately, despite numerous trials in various conditions, we never managed to isolate the attempted compound **7**. During the purification of the reaction mixture by column chromatography on silica gel, compound **7** quickly led to iminoquinone **7a** which was in part

converted into para-quinone **7b**. Conversion of aromatic nitro derivatives to mixtures of corresponding iminoquinone and para-quinone after reduction/oxidation/acidic hydrolysis sequence was previously observed by Fagan *et al.* for imidazo[5,4-*f*]benzimidazoles [24]. Separation of both compounds was tiedous and no pure fraction was isolated. Therefore, we try to completely convert iminoquinone **7a** to para-quinone derivative **7b** in the presence of Fremy's salt. Contrarily to what was described for the imidazo[5,4-*f*]benzimidazoles series, this oxidation reaction was unsuccessful. After many attempts to obtain para-quinone **7b** in acceptable yields, we were only able to get a small sample of pure para-quinone **7b** which was also poorly soluble.

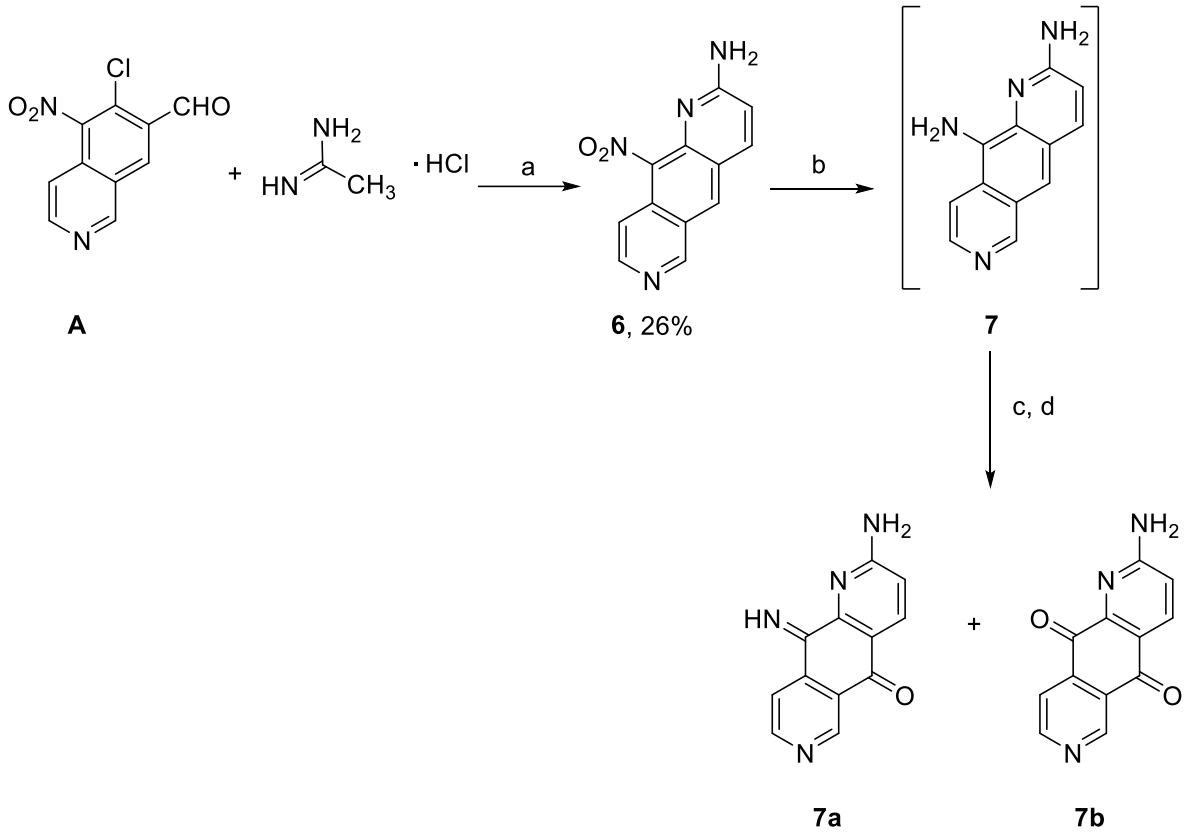

Scheme 2. Synthesis of pyridoquinoline **6**. Reagents and conditions: (a) 4 Å molecular sieves, K_2CO_3, CH_3CN (b) H_2, Pd/C, CH_2Cl_2/MeOH (c) AcOEt, silica, 2 days or Fremy's salt, aqueous KH_2PO_4 (d) HCl 2M

3. Biological evaluation

First of all, the inhibitory potency of new compounds **2a-h**, **2a'**, **3a-g**, and **4-6** were studied toward a panel of 10 protein kinases: Haspin, CDK9/Cyclin T, GSK-3β, CK1ε, CDK5/p25, Pim1, ABL1, JAK3 (all from human) as well as CLK1 (from *Mus musculus)* and DYRK1A (from *Rattus norvegicus*) (Table 1). The percentage of residual kinase activity was evaluated in the presence of 10 μM and 1 μM compound concentrations. In Table 1, only results obtained with 1 μM compound concentration are indicated. Haspin IC_{50} values were only determined when Haspin residual kinase activity was found inferior to 45% at 1 μM compound concentration. For the most active Haspin inhibitors, additional IC_{50} values were determined

against other potently inhibited protein kinases (*e.g.* CLK1, DYRK1A), allowing the determination of the selectivity profile for the best inhibitors.

Table 1. Percentages of kinase residual activities in the presence of 1 μM compound concentration. Kinase inhibitory activities were assayed in duplicate using the ADP-Glo assay (Promega) in the presence of 10 μM ATP. IC_{50} values in nM (given in parentheses) were determined for Haspin when residual activity was < 45%. For the most active Haspin inhibitors, IC_{50} values were determined against other potently inhibited protein kinases (CLK1, DYRK1A and CDK9). Haspin/CLK1 selectivity index (SI) = IC_{50} CLK1 / IC_{50} Haspin. CHR-6494, a potent Haspin inhibitor, was used as a positive control [4].

Cpd	% residual activity (IC_{50} (nM))										SI
	Haspin	CLK1	DYRK1A	CDK9	GSK3	CK1	CDK5	PIM1	ABL1	JAK3	
2a	0 (119)	8 (221)	45 (916.3)	33 (406.8)	68	83	90	85	84	93	1.9
2a'	76	80	68	59	95	96	85	79	65	76	
2b	24 (91)	0 (148)	39 (515)	77	78	96	100	100	71	100	1.6
2c	26 (169)	9	55	57	75	86	95	100	75	90	
2d	35 (114)	12	67	63	73	89	100	96	49	86	
2e	34 (1041)	34	52	59	47	80	100	100	63	73	
2f	30 (484)	34	78	46	50	81	100	100	60	72	
2g	46	64	57	71	71	98	97	100	67	47	
2h	34 (897)	48	100	41	29	87	93	88	87	63	
3a	0 (12)	16 (37)	9 (47)	24 (189)	61	77	55	53	55	56	3.1
3b	20 (124)	24	38	74	41	96	86	97	64	49	
3c	8 (65)	22 (90)	28 (148)	40	57	78	65	38	86	79	1.4
3d	23 (56)	0 (72)	29 (594)	58	65	86	76	82	87	78	1.3
3[e]	14 (69)	0 (92)	13 (132)	49	78	85	100	95	63	100	1.3
3f	18 (202)	3	36	62	72	97	82	87	66	100	

3g	38 (432)	14	23	75	74	89	95	95	61	77	
4	23 (50)	34 (445)	49 (917)	59	76	95	100	100	82	95	8.9
5	14 (159)	8	3	9	80	96	89	62	87	100	
6	3 (3)	13 (20)	15 (87)	9 (24)	29 (418)	55	42	91	94	42	6.7
CHR-6494	2 (3)	0 (8)	6 (13)	12 (29)	10 (53)	6 (99)	35 (41)	20 (29)	13 (162)	19 (119)	2.7

The results obtained indicated that the most inhibited kinases were Haspin, CLK1, DYRK1A and CDK9. Best Haspin inhibitors were **2a-b**, **2d**, **3a, 3c-e**, **4** and **6** showing that all upper heteroaromatic rings studied (alkylsulfanylpyrimidine, methoxypyrimidine, aminopyridine) were able to achieve kinase inhibitions. Particularly, compounds **3a** and **6** exhibited low nanomolar Haspin inhibitory potencies. Compound **2a'** lacking the 10-nitro/amino group was much less active compared to its **2a/3a** analogs, demonstrating again the importance of a 10-nitro/amino group for the kinase inhibitory activity in this series (this was already shown in the aminopyrimidine series [16]). In general, except for **2a** and **6** for which CDK9 was more potently inhibited than DYRK1A, the inhibitory potencies of most active compounds could be classified in the following order: Haspin > CLK1 > DYRK1A > CLK9. To get an insight into the selectivity profile of best Haspin inhibitors, we determined their selectivity index *vs* CLK1 (Table 1). Thiopyrimidine derivatives **2a**, **3a** as well as methoxypyrimidine **4** and pyridoquinoline **6** exhibited selectivity indexes ($1.9 < SI < 8.9$) in favor of Haspin. Note that CHR6494, used as a positive control, displayed very poor overall selectivity toward Haspin as previously reported [25].

In order to further study the selectivity profile of our compounds, we performed a kinase screen toward a larger panel of 486 kinases with compound **4** which appeared to be the most promising molecule in our assays, due to its higher selectivity index (SelectScreen Kinase Profiling Services—Thermo Fisher Scientific, Madison, WI, USA).

Compound **4** was first tested at 10 µM on the full kinase panel (see supplementary information for kinase list and results, Table S1) using either a binding assay (LanthaScreen TR-FRET technology) or two activity assays (Z'-LYTE or Adapta). The screening revealed that 60 out of 486 (12%) kinases had their activity inhibited ≥ 80% at 10 µM (Supplementary Table S1).

In a second step, compound **4** was re-evaluated at 1 µM against the 56 wild-type kinases inhibited more than 80% in terms of activity or binding (Fig. 2A, B). The results obtained showed that, in addition to Haspin, compound **4** inhibited the activity by more than 80% of four additional kinases (Fig. 2A) and affected the ATP-tracer binding for seven other kinases (Fig. 2B). Overall, combined activity and binding assay results showed that only a few kinase families were targeted by compound **4**; in addition to CLKs and DYRKs kinase family, DAPKs (Death-Associated Protein Kinases) and very interestingly PLKs (Polo Like Kinases) family (involved in cell cycle progression and mitosis) were inhibited.

Additionally, we determined the IC_{50} when kinases activity was inhibited by more than 80% (10-point titration, ThermoFisher) (Fig. 2C). The IC_{50} for Haspin was found at 65.8 nM, confirming our previous determination (50 nM) with a different assay. This slight difference can be attributed to the ATP concentrations used (10 µM for our in-lab assay, 25 µM for ThermoFisher assay). The IC_{50} values for PLK1, PLK2, and PLK3 were at 294 nM, 125 nM, and 117 nM, respectively, while the IC_{50} for DAPK3 was even higher at 578 nM.
Overall, these results show that only a few kinases were affected by compound **4** at a level close to Haspin (2.9% of all wild type kinases tested), Haspin remaining the most affected kinase, supporting a very respectable selectivity profile.

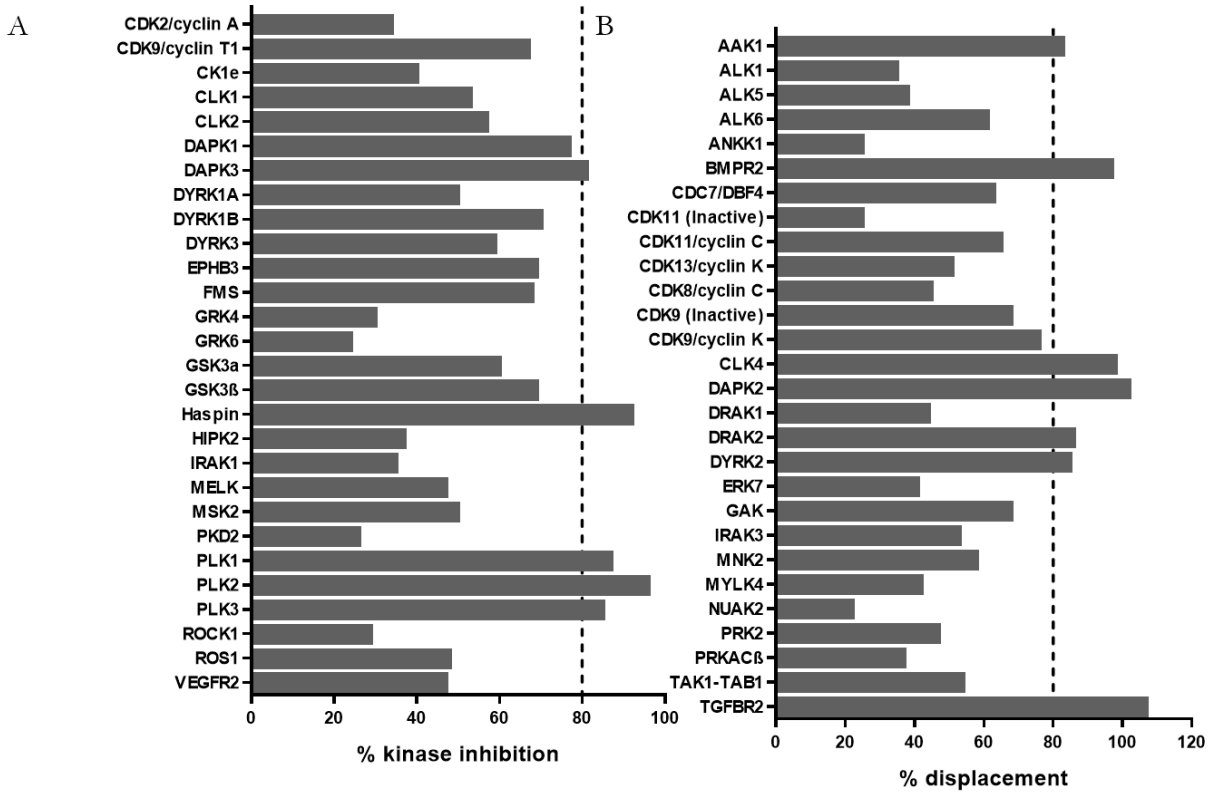

C

	IC_{50} (nM)
Haspin	65.8
PLK1	294
PLK2	125
PLK3	117
DAPK3	578

Figure 2. Kinase inhibition profile of compound **4**. Kinome scan assays were performed for compound **4** (1 µM) against 56 kinases. (A) Z'-Lyte or Adapta activity assay showing the % of inhibition, (B) Lantha Screen Binding assay showing the % of Tracer displacement (see Material & method section for details). (C) IC_{50} calculated for compound **4** on the 5 kinases showing inhibition greater than 80 % on panel A. IC_{50}s were evaluated using ATP concentrations corresponding to the Km of each kinase. A full table of the kinase inhibition profile of compound **4** at 10 µM is available in Supplementary Table S1.

Next, the effect of **2a**, **4** and **6** were evaluated on cancerous and non-cancerous cells, grown as monolayers, in terms of cell viability in a dose-dependent manner. Cell viability was assessed on the following human cancerous cell lines: U-2 OS (osteosarcoma), HCT116 (colorectal cancer), HBL-100 (breast cancer), SH-SY5Y (neuroblastoma) and non-cancerous hTERT-RPE-1 (retinal fibroblast immortalized with hTERT). EC_{50} were calculated from the dose-response curves and shown on Table 2. All cell lines appeared equally sensitive to the tested compounds whether they were of cancerous or non-cancerous origin. Compound **4** showed a moderate activity on cell viability of all tested cell lines while **2a** and **6** showed more cytotoxicity with EC_{50} as low as 0.8 μM for compound **2a** on RPE1 and 0.2 μM for compound **6** on HCT116 and SH-SY5Ycells.

Table 2. Effects of **2a**, **4** and **6** on the viability of cancer and non-cancer cells (EC_{50}, μM). Cells were incubated with increasing doses of each compound (up to 50 μM). Cell viability was determined after 48 h incubation by MTS assay in triplicate were calculated from the dose-response curves.

	hTERT-RPE1	HCT116	SH-SY5Y	U-2 OS	HBL-100
2a	0.8	1.1	1.2	0.9	1.3
4	3.2	6.2	4.4	5.8	8.5
6	0.4	0.2	0.2	0.3	0.8

We further assessed the effect of compounds **2a**, **4** and **6** alongside known Haspin inhibitor CHR-6494 on U-2 OS and HCT116 cancerous cells growing in 3D spheroids. Spheroids were treated for 7 days with increasing concentrations of each compound (1, 5 and 10 μM) after which cell viability was measured. We observed (Fig. 3) a strong dose-dependent effect of the three tested compounds on both U-2 OS and HCT116 spheroids. U-2 OS spheroids appeared more sensitive than HCT116 to the compounds. Compound **6** was found relatively cytotoxic on both types of spheroids, supporting the results obtained on cells grown as monolayers. This result supports the idea that compound **6** may have one or several off-targets strongly affecting cell viability. Overall, these cell viability results, on both 2D and 3D cultures, showed that compound **2a** and **4** displayed moderate, yet interesting inhibitory effects on the growth of several cancerous cell lines.

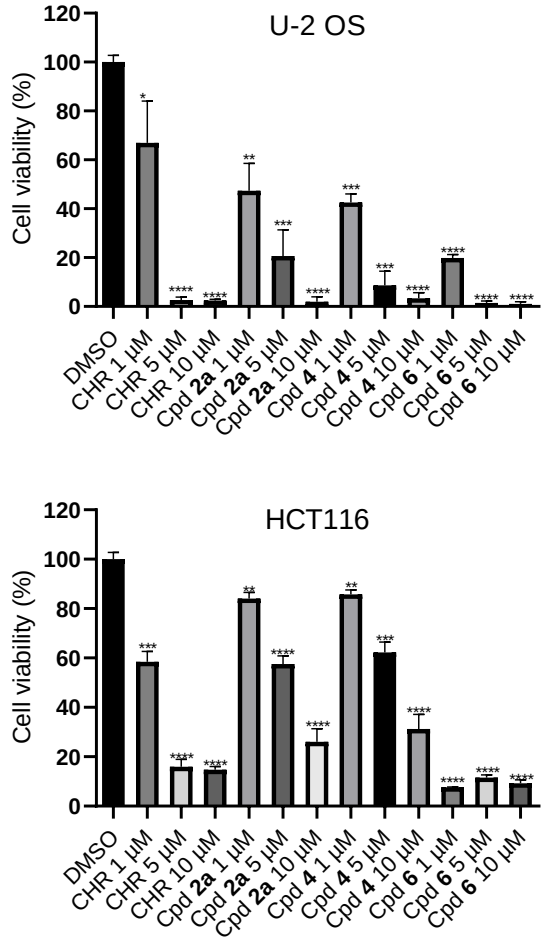

Figure 3. Effects of compounds on spheroid viability. Cell viability in spheroids from U-2 OS and HCT116 cells was measured after 7 days of treatment with 0.5% DMSO, CHR-6494 or compounds **2a**, **4** and **6** at 1, 5 and 10 µM. Cell viability was expressed in percentage of the DMSO control set at 100%. Data were acquired in triplicates, results are mean ± SEM, ****$p < 0.0001$, ***$p \leq 0.0005$, **$p \leq 0.05$, *$p \leq 0.05$ (two-tailed unpaired t-test).

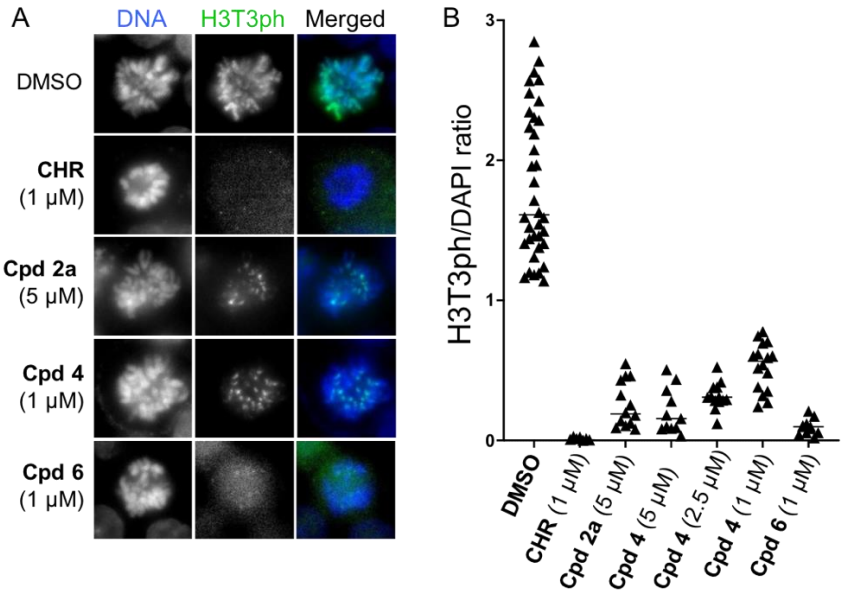

Figure 4. Inhibition of cellular endogenous Haspin activity. HCT116 cells were treated for 16 h with compound **2a** (1 µM), **6** (1 µM), **4** (5, 2.5 and 1 µM), **CHR** (CHR-6494, 1 µM) or 0.1 % **DMSO**. Haspin activity was visualized by immunofluorescence staining of phosphorylated Histone H3 on threonine 3 (H3T3ph, green) and DNA was stained with DAPI (blue). (A) Representative images of cells in prometaphase. (B) Quantification of Haspin activity in prometaphase cells by measuring the H3T3ph and DAPI signals and representing the ratio H3T3ph/DAPI on a scatter plot, n≥15.

In order to assess the ability of our compounds to inhibit Haspin in its cellular context, we treated HCT116 cells with compound **2a** (1 µM), **4** (5, 2.5 and 1 µM), **6** (1 µM), CHR-6494, or 0.1 % of **DMSO** for 16 h (Fig. 4). We assessed cellular endogenous Haspin activity by immunofluorescence, quantifying the phosphorylation of Histone H3 on threonine 3, an Haspin activity specific marker. The H3T3ph and DAPI (DNA) signals were measured on prometaphase cells and the ratio H3T3ph/DAPI is showed on Fig. 4B. The results showed that all four compounds inhibited Haspin activity in HCT116 cells and compound **4** showed a dose-dependent inhibition. These results validated the activity of compound **4** on endogenous Haspin kinase in HCT116 cells.

4. Structural analysis of the binding mode of compound 2a with Haspin.

To provide insights into the binding mode of these compounds with Haspin, we determined the crystal structure of compound **2a** in complex with Haspin at 2.4 Å resolution (Fig. 5). The tricyclic system bound to the ATP-binding site with the pyridine ring oriented toward the hinge region, allowing a hydrogen bond with the hinge GLY608 backbone amine. The thiopyrimidine moiety pointed toward the conserved VAIK motif lysine LYS511, but did not form any specific interaction. Stabilization of compound **2a** in the ATP site of Haspin might likely be achieved through hydrophobic interactions within the back pocket, where its heterocyclic ring was sandwiched between VAL498 and ILE686 residues.

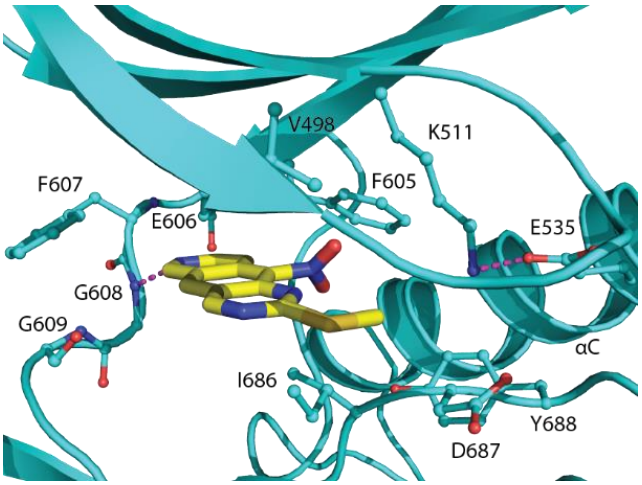

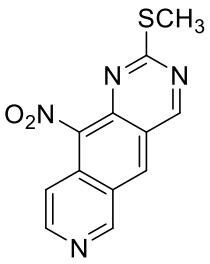

2a

Figure 5. Structure of **2a** bound to Haspin (pdb code: 7OPS). Image produced using Chimera software [26].

5. Conclusion

In summary, we synthesized a series of tricyclic derivatives containing various heteroaromatic rings (thiopyrimidine, methoxypyrimidine, aminopyridine) in the upper part. Altogether, the results obtained demonstrated that pyridoquinazolines bearing at the 2-position an alkyl(thio)ether substituent (**2**, **3**, **4**) and pyridoquinoline (**6**) represent a novel family of kinase inhibitors targeting Haspin kinase. Most interesting derivative **4** demonstrated kinase inhibitory potencies in the nanomolar range in favor of Haspin (inhibition of Haspin > CLK1 > DYRK1A and CDK9) with good selectivity index. This selectivity has been further validated for compound **4** on a large panel of 486 kinases. Interestingly, this kinome scan revealed that the mitotic Polo-kinases are secondary targets of compound **4**. Besides, we further validated the inhibitory activity of our compound **4** on the activity of endogenous cellular Haspin kinase.
In addition, the molecular binding mode of compound **2a** within Haspin was determined giving valuable structural data to further optimize this series.

6. Experimental section

6.1 Chemistry

6.1.1. General. Starting materials were obtained from commercial suppliers and used without further purification. IR spectra were recorded on a Perkin-Elmer Spectrum 65 FT-IR or a Perkin-Elmer Two FT-IR spectrometer ($\bar{\nu}$ in cm^{-1}). NMR spectra, performed on a Bruker AVANCE 400 III HD (^{1}H: 400 MHz, ^{13}C: 101 MHz) are reported in ppm using the solvent residual peak as an internal standard; the following abbreviations are used: singlet (s), doublet (d), triplet (t), quadruplet (q), quintuplet (quint), hexuplet (hex), heptuplet (hept), multiplet (m), broad signal (br s). Coupling constants are expressed in Hertz. Experiments under microwave irradiation were performed using a CEM Discover Benchmate apparatus. High resolution mass spectra were determined on a high-resolution Waters Micro Q-Tof or Thermo Scientific Q Exactive Q-Orbitrap apparatus (UCA START, Université Clermont Auvergne, Clermont-Ferrand, France). Chromatographic purifications were performed by column chromatography

using 40–63 µm silica gel. Reactions were monitored by TLC using fluorescent silica gel plates (60 F254 from Macherey Nagel). Melting points were measured on a Stuart SMP3 apparatus and are uncorrected.
The purity of compounds **2a-2h, 3a-3g** and **6-7** was established by HPLC analysis using a VWR Hitachi chromatograph with DAD detector and an Macherey Nagel Nucleodur gravity column (4.6 mm x 250 mm, 5 µm). Flow rate was 0.5 mL/min and the analysis was performed at 25 °C at 295 nm as detection wavelength for each compound. Solvents were (A) water/0.1% formic acid, (B) acetonitrile. Two methods were designed: method A was a gradient 5:95 A/B for 5 min to 95:5 A/B in 45 min whereas method B was an isocratic mode using 50/50 water/acetonitrile.

6.1.2. General procedure for the synthesis of compounds 2a-h:

To a solution of 70 mg (0.296 mmol) of 6-chloro-5-nitroisoquinoline-7-carbaldehyde **A** in 1.4 mL of *N*,*N*-dimethylacetamide were successively added 0.592 mmol of isothiouronium salts **1a-h** and 50 mg (0.592 mmol) of sodium hydrogenocarbonate. Argon was bubbled through the solution for 20 min at room temperature. Temperature was then raised to 120 °C and the reaction mixture was stirred at this temperature for additional 20-30 min (until complete disappearance of carbaldehyde on TLC). The reaction was poured in 200 mL EtOAc and the organic phase was washed with 200 mL water and 50 mL of saturated NaCl solution. The assembled organic phases were dried over $MgSO_4$ and concentrated under reduced pressure. The residue was purified by flash column chromatography using a gradient of CH_2Cl_2/Acetone 95:5 to 90:10.

2-(Methylsulfanyl)-10-nitropyrido[3,4-g]quinazoline (2a), obtained as an orange yellow solid in 45% yield (36 mg, 0.132 mmol). Mp: 253-254 °C. R_f = 0.15 (CH_2Cl_2/Acetone 95:5). IR (ATR): 2923, 1622, 1597, 1563, 1523, 1366, 1124 cm^{-1}. ^1H NMR (400 MHz, DMSO-d_6) δ 2.62 (3H, s), 7.82 (1H, d, *J* = 6.0 Hz), 8.75 (1H, d, *J* = 6.0 Hz), 9.39 (1H, s), 9.80 (1H, s), 9.84 (1H, s). ^{13}C NMR (100 MHz, DMSO-d_6) δ 14.0 (CH_3), 113.0, 135.6, 146.7, 155.7, 163.5 (CH_{arom}), 120.8, 124.6, 128.1, 137.9, 138.7, 173.0 (C_{arom}).HRMS (ESI+) calcd for $C_{12}H_9N_4O_2S$ $(M + H)^+$ 273.0446, found 273.0463. HPLC method A: purity > 99%, λ = 295 nm, t_R = 24.8 min.

2,10-Bis(methylsulfanyl)pyrido[3,4-g]quinazoline (2a'), obtained as an orange yellow solid in 14% yield (11 mg, 0.041 mmol). Mp: 175-176 °C R_f = 0.25 (EtOAc/Cyclohexane 1:2). IR (ATR): 2917, 1610, 1586, 1527, 1361, 1170, 1110 cm^{-1}. ^1H NMR (400 MHz, DMSO-d_6) δ 2.59 (3H, s), 2.69 (3H, s), 8.07 (1H, d, *J* = 5.6 Hz), 8.54 (1H, s), 8.62 (1H, d, *J* = 5.6 Hz), 10.16 (2H, s). Due to poor solubility, spectrum was also recorded in Acetone-d_6: ^1H NMR (400 MHz, Acetone-d_6) δ 2.65 (3H, s), 2.71 (3H, s), 8.01 (1H, d, *J* = 6.0 Hz), 8.47 (1H, s), 8.61 (1H, d, *J* = 6.0 Hz), 10.20 (1H, s), 10.25 (1H, s). ^{13}C NMR spectrum for **2a'**.HCl (100 MHz, Acetone-d_6/D_2O 5:1 + 2 drops HCl 1N) δ 14.3, 21.4 (CH_3), 114.9, 126.2, 133.7, 146.8, 162.4 (CH_{arom}), 127.9, 131.4, 139.2, 140.6, 141.4, 166.7 (C_{arom}). HRMS (ESI+) calcd for $C_{13}H_{12}N_3S_2$ $(M + H)^+$ 274.0473, found 274.0463. HPLC method A: purity > 97%, λ = 270 nm, t_R = 18.3 min.

2-(Ethylsulfanyl)-10-nitropyrido[3,4-g]quinazoline (2b), obtained as an orange yellow solid in 28% yield (24 mg, 0.084 mmol). Mp: 186-187 °C. R_f = 0.15 (CH_2Cl_2/Acetone 95:5) or 0.45

(EtOAc). IR (ATR): 2934, 1623, 1597, 1560, 1520, 1366, 1340, 1118 cm^{-1}. ^1H NMR (400 MHz, DMSO-d_6) δ 1.39 (3H, t, *J* = 6.8 Hz), 3.19 (2H, q, *J* = 6.8 Hz), 7.82 (1H, d, *J* = 6.0 Hz), 8.74 (1H, d, *J* = 6.0 Hz), 9.38 (1H, s), 9.80 (1H, s), 9.83 (1H, s). ^{13}C NMR (100 MHz, DMSO-d_6) δ 13.8 (CH_3), 25.4 (CH_2), 113.0, 135.6, 146.6, 155.6, 163.6 (CH_{arom}), 120.7, 124.6, 128.0, 138.1, 138.6, 172.5 (C_{arom}). HRMS (ESI+) calcd for $C_{13}H_{11}N_4O_2S$ $(M + H)^+$ 287.0597, found 287.0585. HPLC method A: purity > 98%, λ = 295 nm, t_R = 26.2 min.

2-(Propylsulfanyl)-10-nitropyrido[3,4-g]quinazoline (2c), obtained as a yellow solid in 32% yield (28 mg, 0.093 mmol). Mp: 145-146 °C. R_f = 0.45 (EtOAc). IR (ATR): 2928, 1628, 1599, 1566, 1532, 1361, 1123 cm^{-1}. ^1H NMR (400 MHz, DMSO-d_6) δ 1.02 (3H, t, *J* = 7.2 Hz), 1.75 (2H, hex, *J* = 7.2 Hz), 3.17 (2H, t, *J* = 7.2 Hz), 7.81 (1H, d, *J* = 6.0 Hz), 8.74 (1H, d, *J* = 6.0 Hz), 9.36 (1H, s), 9.79 (1H, s), 9.82 (1H, s). ^{13}C NMR (100 MHz, DMSO-d_6) δ 13.2 (CH_3), 21.8, 32.7 (CH_2), 112.9, 135.5, 146.6, 155.6, 163.5 (CH_{arom}), 120.7, 124.5, 128.0, 137.9, 138.6, 172.6 (C_{arom}). HRMS (ESI+) calcd for $C_{14}H_{13}N_4O_2S$ $(M + H)^+$ 301.0754, found 301.0768. HPLC method A: purity > 98%, λ = 295 nm, t_R = 28.6 min.

2-(1-Methylethylsulfanyl)-10-nitropyrido[3,4-g]quinazoline (2d), obtained as an orange yellow solid in 36% yield (32 mg, 0.107 mmol). Mp: 170-172 °C. R_f = 0.45 (EtOAc). IR (ATR): 2968, 1625, 1596, 1561, 1365, 1341, 1122 cm^{-1}. ^1H NMR (400 MHz, DMSO-d_6) δ 1.46 (6H, d, *J* = 6.8 Hz), 3.89 (1H, hept, *J* = 6.8 Hz), 7.83 (1H, d, *J* = 6.4 Hz), 8.75 (1H, d, *J* = 6.4 Hz), 9.38 (1H, s), 9.80 (1H, s), 9.83 (1H, s). ^{13}C NMR (100 MHz, DMSO-d_6) δ 21.9 ($2CH_3$), 36.5 (CH), 113.0, 135.5, 146.6, 155.6, 163.5 (CH_{arom}), 120.7, 124.6, 128.0, 138.1, 138.6, 172.4 (C_{arom}). HRMS (ESI+) calcd for $C_{14}H_{13}N_4O_2S$ $(M + H)^+$ 301.0754, found 301.0756. HPLC method A: purity > 99%, λ = 295 nm, t_R = 28.2 min.

2-(Butylsulfanyl)-10-nitropyrido[3,4-g]quinazoline (2e), obtained as an orange yellow solid in 51% yield (47 mg, 0.150 mmol). Mp: 133-135 °C. R_f = 0.45 (EtOAc). IR (ATR): 2926, 1626, 1564, 1540, 1519, 1366, 1128 cm^{-1}. ^1H NMR (400 MHz, DMSO-d_6) δ 0.94 (3H, t, *J* = 7.2 Hz), 1.45 (2H, hex, *J* = 7.2 Hz), 1.73 (2H, quint, *J* = 7.2 Hz), 3.19 (2H, t, *J* = 7.2 Hz), 7.81 (1H, d, *J* = 6.4 Hz), 8.75 (1H, d, *J* = 6.4 Hz), 9.37 (1H, s), 9.80 (1H, s), 9.83 (1H, s). ^{13}C NMR (100 MHz, DMSO-d_6) δ 13.4 (CH_3), 21.5, 30.47, 30.49 (CH_2), 113.0, 135.5, 146.6, 155.6, 163.5 (CH_{arom}), 120.7, 124.6, 128.0, 138.1, 138.6, 172.6 (C_{arom}). HRMS (ESI+) calcd for $C_{15}H_{15}N_4O_2S$ $(M + H)^+$ 315.0910, found 315.0896. HPLC method A: purity > 99%, λ = 295 nm, t_R = 30.9 min.

2-(1-Methylpropylsulfanyl)-10-nitropyrido[3,4-g]quinazoline (2f), obtained as an orange yellow solid in 58% yield (54 mg, 0.172 mmol). Mp: 159-161 °C. R_f = 0.45 (EtOAc). IR (ATR): 2924, 1627, 1597, 1561 1538, 1518, 1342, 1119 cm^{-1}. ^1H NMR (400 MHz, DMSO-d_6) δ 1.02 (3H, t, *J* = 7.2 Hz), 1.44 (3H, d, *J* = 6.8 Hz), 1.70-1.85 (2H, m), 3.78 (1H, hex, *J* = 6.8 Hz), 7.82 (1H, d, *J* = 6.4 Hz), 8.74 (1H, d, *J* = 6.4 Hz), 9.37 (1H, s), 9.80 (1H, s), 9.82 (1H, s). ^{13}C NMR (100 MHz, DMSO-d_6) δ 11.3, 19.4 (CH_3), 28.5 (CH_2), 42.7 (CH), 113.0, 135.4, 146.6, 155.6, 163.5 (CH_{arom}), 120.7, 124.6, 128.0, 138.0, 138.6, 172.5 (C_{arom}). HRMS (ESI+) calcd for $C_{15}H_{15}N_4O_2S$ $(M + H)^+$ 315.0910, found 315.0921. HPLC method A: purity > 96%, λ = 295 nm, t_R = 30.4 min.

2-(Pentylsulfanyl)-10-nitropyrido[3,4-g]quinazoline (2g), obtained as an orange yellow solid in 58% yield (56 mg, 0.171 mmol). Mp: 110-111 °C. R_f = 0.45 (EtOAc). IR (ATR): 2925, 1624, 1599, 1565, 1526, 1345, 1119 cm^{-1}. ^1H NMR (500 MHz, DMSO-d_6) δ 0.89 (3H, t, *J* = 7.0 Hz), 1.13-1.35 (4H, m), 1.72 (2H, quint, *J* = 7.5 Hz), 3.17 (2H, t, *J* = 7.5 Hz), 7.79 (1H, d, *J* = 6.0 Hz), 8.73 (1H, d, *J* = 6.0 Hz), 9.34 (1H, s), 9.77 (1H, s), 9.80 (1H, s). ^{13}C NMR (100 MHz, DMSO-d_6) δ 13.9 (CH_3), 21.7, 28.2, 30.6, 30.8 (CH_2), 113.0, 135.5, 146.6, 155.6, 163.5 (CH_{arom}), 120.7, 124.6, 128.0, 138.0, 138.6, 172.6 (C_{arom}). HRMS (ESI+) calcd for $C_{16}H_{17}N_4O_2S$ $(M + H)^+$ 329.1067, found 329.1062. HPLC method A: purity > 99%, λ = 295 nm, t_R = 33.1 min.

Ethyl 3-((10-nitropyrido[3,4-g]quinazolin-2-yl)thio)propanoate (2h), obtained as an orange yellow solid in 10% yield (10.6 mg, 0.030 mmol). Mp: 86-87 °C. R_f = 0.50 (EtOAc). IR (ATR): 2926, 1723, 1627, 1564, 1529, 1346, 1123 cm^{-1}. ^1H NMR (500 MHz, DMSO-d_6) δ 1.21 (3H, t, *J* = 7.0 Hz), 2.85 (2H, t, *J* = 7.0 Hz), 3.38 (2H, t, *J* = 7.0 Hz), 4.12 (2H, q, *J* = 7.0 Hz), 7.82 (1H, d, *J* = 6.5 Hz), 8.74 (1H, d, *J* = 6.5 Hz), 9.38 (1H, s), 9.79 (1H, s), 9.84 (1H, s). ^{13}C NMR (100 MHz, DMSO-d_6) δ 14.1 (CH_3), 26.2, 32.7, 60.2 (CH_2), 113.0, 135.7, 146.7, 155.7, 163.8 (CH_{arom}), 120.8, 124.7, 128.1, 138.0, 138.7, 171.3, 172.0 (C_{arom}). HRMS (ESI+) calcd for $C_{16}H_{15}N_4O_4S$ $(M + H)^+$ 359.0809, found 359.0803. HPLC method A: purity > 95%, λ = 295 nm, t_R = 26.1 min.

6.1.3. General procedure for the synthesis of compounds 3a-g:

To a solution of 0.107 mmol of tricyclic derivatives **2a-g** in 1.8 mL of MeOH/H_2O 2:1 were added 5 eq of iron powder and 4 eq of ammonium chloride. The suspension was stirred at 80 °C for 18-40 h. After a filtration over a Celite® pad and washings with EtOAc and water, both phases were transferred in a separating funnel. The desired product was extracted with EtOAc. Combined organic phases were washed with brine, dried over $MgSO_4$ and concentrated under reduced pressure. The residue was purified by flash column chromatography using a gradient of CH_2Cl_2/MeOH 99:1 to 98.5:1.5

2-(Methylsulfanyl)pyrido[3,4-g]quinazolin-10-amine (3a), obtained as a dark red solid in 22% yield (5.8 mg, 0.024 mmol). Mp: 69-70 °C. R_f = 0.70 (CH_2Cl_2/EtOH 95:5). IR (ATR): 3430-2547, 2922, 1632, 1538, 1461, 1404, 1209, 1098 cm^{-1}. ^1H NMR (500 MHz, DMSO-d_6) δ 2.71 (3H, s), 6.92 (2H, br s), 7.97 (1H, s), 8.23 (1H, d, *J* = 6.0 Hz), 8.37 (1H, d, *J* = 6.0 Hz), 9.39 (1H, s), 9.51 (1H, s). ^{13}C NMR (100 MHz, DMSO-d_6) δ 14.0 (CH_3), 112.4, 115.8, 140.1, 154.7, 162.9 (CH_{arom}), 121.2, 121.7, 126.6, 132.5, 139.1, 164.5 (C_{arom}). HRMS (ESI+) calcd for $C_{12}H_{11}N_4S$ $(M + H)^+$ 243.0699, found 243.0696. HPLC method B: purity > 96%, λ = 240 nm, t_R = 5.9 min.

2-(Ethylsulfanyl)pyrido[3,4-g]quinazolin-10-amine (3b), obtained as a dark red oil in 14% yield (3.8 mg, 0.015 mmol). R_f = 0.65 (CH_2Cl_2/EtOH 95:5). IR (ATR): 3378-2767, 2922, 1617, 1589, 1539, 1404, 1357, 1096 cm^{-1}. ^1H NMR (500 MHz, DMSO-d_6) δ 1.41 (3H, t, *J* = 7.5 Hz), 3.34 (2H, q, *J* = 7.5 Hz), 6.88 (2H, br s), 7.96 (1H, s), 8.22 (1H, d, *J* = 6.0 Hz), 8.36 (1H, d, *J* = 6.0 Hz), 9.38 (1H, s), 9.51 (1H, s). ^{13}C NMR (100 MHz, DMSO-d_6) δ 14.1 (CH_3), 24.7 (CH_2), 112.5, 115.8, 140.1, 154.7, 163.1 (CH_{arom}), 121.2, 121.6, 126.6, 132.5, 139.0, 163.9 (C_{arom}).

HRMS (ESI+) calcd for $C_{13}H_{13}N_4S$ $(M + H)^+$ 257.0855, found 257.0850. HPLC method B: purity > 95%, λ = 240 nm, t_R = 9.7 min.

2-(Propylsulfanyl)pyrido[3,4-g]quinazolin-10-amine (3c), obtained as a red oil in 17% yield (5 mg, 0.018 mmol). R_f = 0.65 (CH_2Cl_2/EtOH 95:5). IR (ATR): 3531-2453, 2923, 1667, 1589, 1557, 1294, 1114 cm^{-1}. ^1H NMR (500 MHz, DMSO-d_6) δ 1.06 (3H, t, *J* = 7.0 Hz), 1.78 (2H, hex, *J* = 7.0 Hz), 3.33 (2H, t, *J* = 7.0 Hz), 6.86 (2H, br s), 7.96 (1H, s), 8.21 (1H, d, *J* = 6.0 Hz), 8.37 (1H, d, *J* = 6.0 Hz), 9.39 (1H, s), 9.51 (1H, s). ^{13}C NMR (125 MHz, DMSO-d_6) δ 13.4 (CH_3), 22.0, 32.2 (CH_2), 112.5, 115.8, 140.1, 154.7, 163.0 (CH_{arom}), 121.2, 121.6, 126.6, 132.5, 138.9, 164.1 (C_{arom}). HRMS (ESI+) calcd for $C_{14}H_{15}N_4S$ $(M + H)^+$ 271.1012, found 271.1008. HPLC method B: purity > 96%, λ = 240 nm, t_R = 8.1 min.

2-(1-Methylethylsulfanyl)pyrido[3,4-g]quinazolin-10-amine (3d), obtained as a dark red oil in 27% yield (8 mg, 0.029 mmol). R_f = 0.65 (CH_2Cl_2/EtOH 95:5). IR (ATR): 3406-2827, 2923, 1669, 1558, 1294, 1115 cm^{-1}. ^1H NMR (500 MHz, DMSO-d_6) δ 1.46 (6H, d, *J* = 7.0 Hz), 4.21 (1H, hept, *J* = 7.0 Hz), 6.86 (2H, br s), 7.95 (1H, s), 8.21 (1H, d, *J* = 6.5 Hz), 8.36 (1H, d, *J* = 6.0 Hz), 9.38 (1H, s), 9.50 (1H, s). ^{13}C NMR (100 MHz, DMSO-d_6) δ 22.5 ($2CH_3$), 35.3 (CH), 112.5, 115.8, 140.0, 154.7, 163.1 (CH_{arom}), 121.2, 121.6, 126.6, 132.6, 139.0, 163.9 (C_{arom}). HRMS (ESI+) calcd for $C_{14}H_{15}N_4S$ $(M + H)^+$ 271.1012, found 271.1004. HPLC method B: purity > 99%, λ = 240 nm, t_R = 8.0 min.

2-(Butylsulfanyl)pyrido[3,4-g]quinazolin-10-amine (3e), obtained as a dark red solid in 34% yield (10.2 mg, 0.036 mmol). Mp: 98-99 °C. R_f = 0.60 (CH_2Cl_2/EtOH 95:5). IR (ATR): 3361-2612, 2924, 1625, 1540, 1452, 1405, 1364, 1271, 1098 cm^{-1}. ^1H NMR (500 MHz, DMSO-d_6) δ 0.95 (3H, t, *J* = 7.0 Hz), 1.46 (2H, hex, *J* = 7.0 Hz), 1.74 (2H, quint, *J* = 7.0 Hz), 3.34 (2H, t, *J* = 7.5 Hz), 6.86 (2H, br s), 7.97 (1H, s), 8.20 (1H, d, *J* = 6.0 Hz), 8.37 (1H, d, *J* = 6.0 Hz), 9.39 (1H, s), 9.51 (1H, s). ^{13}C NMR (125 MHz, DMSO-d_6) δ 13.6 (CH_3), 21.6, 30.0, 30.7 (CH_2), 112.6, 115.7, 140.1, 154.7, 163.1 (CH_{arom}), 121.2, 121.7, 126.6, 132.5, 138.9, 164.1 (C_{arom}). HRMS (ESI+) calcd for $C_{15}H_{17}N_4S$ $(M + H)^+$ 285.1168, found 285.1165. HPLC method B: purity > 99%, λ = 240 nm, t_R = 10.7 min.

2-(1-Methylpropylsulfanyl)pyrido[3,4-g]quinazolin-10-amine (3f), obtained as a dark red oil in 39% yield (12 mg, 0.042 mmol). R_f = 0.55 (CH_2Cl_2/EtOH 95:5). IR (ATR): 3403-2771, 2923, 1614, 1535, 1403, 1357, 1293, 1092 cm^{-1}. ^1H NMR (500 MHz, DMSO-d_6) δ 1.05 (3H, t, *J* = 7.0 Hz), 1.45 (3H, d, *J* = 6.5 Hz), 1.71-1.82 (2H, m), 4.14 (1H, hex, *J* = 7.0 Hz), 6.85 (2H, br s), 7.96 (1H, s), 8.21 (1H, d, *J* = 6.5 Hz), 8.37 (1H, d, *J* = 6.5 Hz), 9.39 (1H, s), 9.51 (1H, s). ^{13}C NMR (125 MHz, DMSO-d_6) δ 11.4, 20.2 (CH_3), 28.8 (CH_2), 41.4 (CH), 112.5, 115.7, 140.1, 154.7, 163.0 (CH_{arom}), 121.2, 121.6, 126.6, 132.5, 138.9, 164.1 (C_{arom}). HRMS (ESI+) calcd for $C_{15}H_{17}N_4S$ $(M + H)^+$ 285.1168, found 285.1163. HPLC method B: purity > 97%, λ = 240 nm, t_R = 9.7 min.

2-(Pentylsulfanyl)pyrido[3,4-g]quinazolin-10-amine (3g), obtained as a dark red oil in 58% yield (18.8 mg, 0.063 mmol). R_f = 0.55 (CH_2Cl_2/EtOH 95:5). IR (ATR): 3395-2825, 2922, 1615, 1538, 1405, 1358, 1295, 1097 cm^{-1}. ^1H NMR (500 MHz, DMSO-d_6) δ 0.89 (3H, t, *J* = 7.0 Hz), 1.22-1.35 (2H, m), 1.40-1.46 (2H, m), 1.77 (2H, quint, *J* = 7.5 Hz), 3.33 (2H, t, *J* = 7.5

Hz), 6.87 (2H, br s), 7.97 (1H, s), 8.21 (1H, d, *J* = 6.5 Hz), 8.37 (1H, d, *J* = 6.5 Hz), 9.40 (1H, s), 9.51 (1H, s). ^{13}C NMR (125 MHz, DMSO-d_6) δ 13.9 (CH_3), 21.8, 28.3, 30.3, 30.6 (CH_2), 112.5, 115.7, 140.1, 154.7, 163.1 (CH_{arom}), 121.2, 121.7, 126.6, 132.5, 138.9, 164.1 (C_{arom}). HRMS (ESI+) calcd for $C_{16}H_{19}N_4S$ $(M + H)^+$ 299.1325, found 299.1322. HPLC method B: purity > 98%, λ = 240 nm, t_R = 14.4 min.

6.1.4. 2-Methoxy-10-nitropyrido[3,4-g]quinazoline (4)

To a solution of intermediate **A** (200 mg, 0.845 mmol) and *O*-methylisourea bisulfate (366 mg, 2.113 mmol) in 8 mL CH_3CN were successively added K_2CO_3 (292 mg, 2.113 mmol) and 30-35 molecular sieves beads. The mixture was stirred for 3 h at room temperature and then for 4.5 h at 80 °C. The reaction was filtered over a Celite® pad and washed with EtOAc. After evaporation, the crude mixture was subjected to column chromatography using DCM/MeOH from 99:1 to 98:2. Compound **4** (23.8 mg, 0.093 mmol) was obtained as a yellow solid in 11% yield. Mp: 166-167 °C. R_f = 0.10 (CH_2Cl_2/EtOH 95:5). IR (ATR): 2922, 1631, 1579, 1520, 1385, 1281, 1009 cm^{-1}. ^{1}H NMR (400 MHz, DMSO-d_6) δ 4.08 (3H, s), 7.80 (1H, d, *J* = 6.4 Hz), 8.74 (1H, d, *J* = 6.4 Hz), 9.42 (1H, s), 9.80 (1H, s), 9.97 (1H, s). ^{13}C NMR (100 MHz, DMSO-d_6) δ 55.6 (CH_3), 112.8, 135.4, 146.6, 155.7, 168.4 (CH_{arom}), 120.5, 124.0, 128.1, 138.6, 139.5, 163.9 (C_{arom}). HRMS (ESI+) calcd for $C_{12}H_9N_4O_3$ $(M + H)^+$ 257.0669, found 257.0669. HPLC method B: purity > 95%, λ = 240 nm, t_R = 7.65 min.

6.1.5. 2-Methoxypyrido[3,4-g]quinazolin-10-amine (5)

To a solution of compound **4** (19 mg, 0.075 mmol) in CH_2Cl_2/MeOH 8:2 (2 mL) was added Pd/C (4 mg). The suspension was stirred at room temperature for 2 h 45 under hydrogen atmosphere (balloon). The reaction mixture was filtered over a Celite® pad, EtOAc and MeOH were used for washings. After evaporation, the crude mixture was subjected to column chromatography using DCM/MeOH from 99:1 to 98.5:1.5. Compound **5** (6.7 mg, 0.029 mmol) was obtained as a dark red oil in 39% yield. R_f = 0.20 (CH_2Cl_2/MeOH 95:5). IR (ATR): 3416-2833, 2922, 1603, 1571, 1438, 1367, 1318 cm^{-1}. ^{1}H NMR (400 MHz, DMSO-d_6) δ 4.13 (3H, s), 6.78 (2H, br s), 8.03 (1H, s), 8.18 (1H, d, *J* = 6.4 Hz), 8.34 (1H, d, *J* = 6.4 Hz), 9.39 (1H, s), 9.62 (1H, s). ^{13}C NMR (100 MHz, DMSO-d_6) δ 54.8 (CH_3), 112.8, 115.7, 139.8, 154.8, 167.1 (CH_{arom}), 120.8, 121.3, 126.0, 132.7, 138.6, 160.5 (C_{arom}). HRMS (ESI+) calcd for $C_{12}H_{11}N_4O$ $(M + H)^+$ 227.0927, found 227.0928. HPLC method A: purity > 95%, λ = 270 nm, t_R = 18.2 min.

6.1.6. 10-Nitropyrido[3,4-g]quinoline-2-amine (6)

To a solution of intermediate **A** (70 mg, 0.296 mmol) and acetamidine hydrochloride (39 mg, 0.414 mmol) in 3 mL CH_3CN under argon at room temperature were successively added K_2CO_3 (57 mg, 0.414 mmol) and 8 molecular sieves beads. The mixture was heated overnight at 80 °C. The reaction was filtered over a Celite® pad and washed with EtOAc. After evaporation, the crude mixture was subjected to column chromatography using DCM/MeOH from 98:2 to 95:5. Compound **6** (18.8 mg, 0.078 mmol) was obtained as a yellow solid in 26% yield. Mp: 238-240 °C. R_f = 0.40 (EtOAc). IR (ATR): 3236-2552, 1616, 1498, 1418, 1355, 1285 cm^{-1}. ^{1}H NMR (500 MHz, DMSO-d_6) δ 6.99 (1 H, d, *J* = 9.0 Hz), 7.46 (1 H, d, *J* = 6.5 Hz), 7.70 (2H, br s), 8.24 (1 H, d, *J* = 9.0 Hz), 8.49 (1 H, d, *J* = 6.5 Hz), 8.73 (1H, s), 9.46 (1H, s). ^{13}C NMR (125

MHz, DMSO-d_6) δ 112.0, 116.8, 130.7, 137.5, 144.4, 153.8 (CH_{arom}), 121.7, 124.1, 125.7, 137.2, 140.0, 160.5 (C_{arom}). HRMS (ESI+) calcd for $C_{12}H_9N_4O_2$ $(M + H)^+$ 241.0720, found 241.0714. HPLC method A: purity > 95%, λ = 240 nm, t_R = 19.33 min.

6.1.7. 2-Aminopyrido[3,4-g]quinoline-5,10-dione (*7b*)

To a solution of compound **6** (30 mg, 0.125 mmol) in 5 mL DCM/MeOH (1:1) was added 5 mol% of palladium on charcoal (10% wt, 6.9 mg). The mixture was allowed to stir under 1 atm. H_2 for 3 h. The mixture was then filtered trough Celite®, and the Celite® pad was washed with a mixture of DCM/MeOH (1:1). Combined filtrates were concentrated under reduced pressure to give a mixture of amino compound and iminoquinone as intermediates. This mixture was allowed to stir again for 2 days in ethyl acetate at room temperature to favor the formation of the iminoquinone. A purification by flash chromatography using DCM/MeOH (97:3) as eluent afforded a mixture of iminoquinone and para-quinone (formed through the silica). This mixture was again allowed to stir for 2 days in ethyl acetate. Finally, the para-quinone was isolated through flash chromatography using DCM/MeOH (97:3) as eluent to give a red solid (3 mg, 0.013 mmol) in 11% yield. ^{1}H NMR (400 MHz, DMSO-d_6) δ 6.87 (1H, d, J = 8.8 Hz), 7.59 (2H, br s), 7.96 (1H, d, J = 4.8 Hz), 8.14 (1H, d, J = 8.8 Hz), 9.09 (1H, d, J = 5.2 Hz), 9.30 (1H, s). HRMS (ESI+) calcd for $C_{12}H_8N_3O_2$ $(M + H)^+$ 226.0611, found 226.0608.

6.2 Protein kinase assays

Kinase enzymatic activities were assayed in 384 well plates using the ADP-GloTM assay kit (Promega, Madison, WI, USA) according the manufacturer's guidance [27]. Briefly, the reactions were carried out in a final volume of 6 µL for 30 min at 30 °C in an appropriate kinase buffer (10 mM $MgCl_2$, 1 mM EGTA, 1 mM DTT, 25 mM Tris-HCl pH 7.5, 50 µg/mL heparin), with either protein or peptide as substrate in the presence of 10 µM ATP (40 mM Tris pH 7.5, 20 mM $MgCl_2$ and 0.1 mg/mL of BSA). Afterward, 6 µL of ADP-GloTM Kinase Reagent was added to stop the kinase reaction. After an incubation time of 50 min at room temperature (RT), 12 µL of Kinase Detection Reagent was added for 1 h at RT. The transmitted signal was measured using the Envision (Perkin Elmer, Waltham, MA, USA) microplate luminometer and expressed in relative light unit (RLU). In order to determine the half maximal inhibitory concentration (IC_{50}), the assays were performed in duplicate in the absence or presence of increasing doses of the tested compounds. GraphPad Prism6 software (GraphPad Software, San Diego, CA, USA) was used to fit dose–response curves and to determine the IC_{50} values. Kinase activities are expressed in percentage of maximal activity, i.e., measured in the absence of inhibitor. Peptide substrates were obtained from Proteogenix (Schiltigheim, France).

The following protein kinases were analyzed in this study: ABL1 (human, recombinant, expressed by baculovirus in Sf9 insect cells) was assayed with 0.17 µg/µL of the following peptide: EAIYAAPFAKKK, as substrate; CDK5/p25 (human, recombinant, expressed in bacteria) was assayed with 0.8 µg/µL of histone H1 as substrate; CDK9/CyclinT (human, recombinant, expressed by baculovirus in Sf9 insect cells) were assayed with 0.27 µg/µL of the following peptide: YSPTSPSYSPTSPSYSPTSPSKKKK, as substrate; CK1ε (human, recombinant, expressed by baculovirus in Sf9 insect cells) was assayed with 0.022 µg/µL of the following peptide: RRKHAAIGSpAYSITA ("Sp" stands for phosphorylated serine) as CK1-

specific substrate; GSK3β (human, recombinant, expressed by baculovirus in Sf9 insect cells) were assayed with 0.010 μg/μL of GS-1 peptide, a GSK-3-selective substrate (YRRAAVPPSPSLSRHSSPHQSpEDEEE); Haspin-kd (human, kinase domain, amino acids 470−798, recombinant, expressed in bacteria) was assayed with 0.007 μg/μL of histone H3 (1−21) peptide (ARTKQTARKSTGGKAPRKQLA) as substrate; JAK3 (human, recombinant, expressed by baculovirus in Sf9 insect) was assayed with 0.17 μg/μL of the following peptide: GGEEEEYFELVKKKK, as substrate; Pim-1 (human proto-oncogene, recombinant, expressed in bacteria) was assayed with 0.8 μg/μL of histone H1 as substrate; MmCLK1 (from *Mus musculus*, recombinant, expressed in bacteria) was assayed with 0.027 μg/μL of the following peptide: GRSRSRSRSRSR as substrate; RnDYRK1A-kd (*Rattus norvegicus*, amino acids 1−499 including the kinase domain, recombinant, expressed in bacteria, DNA vector kindly provided by Dr. W. Becker, Aachen, Germany) was assayed with 0.033 μg/μL of the following peptide: KKISGRLSPIMTEQ as substrate.

6.3 SelectScreen Kinase Profiling (Thermo Fisher Scientific, Madison, WI, USA)

This screen utilized three different assays appropriate to each kinase, its substrate, and its activity: a binding assay (LanthaScreen TR-FRET technology) and two activity assays (Z'-LYTE or Adapta).

The LanthaScreen Eu Kinase Binding Assay utilizes an Alexa Fluor conjugated "tracer" and a Eu-labeled anti-tag antibody to measure binding of a compound to the kinase target. The Z'-LYTE Kinase Assay determines the differential sensitivity of phosphorylated and non-phosphorylated peptide substrates using a FRET-based readout. The Adapta Universal Kinase Assay is a fluorescence-based immunoassay for the detection of ADP produced by kinases utilizing the TR-FRET technology. For the activity assays, the used ATP concentrations were set at the approximative Km for each kinase. For more information, see the SelectScreen Kinase Profiling Services on ThermoFisher website.

6.4 Cellular evaluation

6.4.1. Cell culture

HCT116, SH-SY5Y, HBL100, U-2 OS and hTERT RPE-1 cells were cultured in Dulbecco's modified Eagle's medium (DMEM) supplemented with 10% fetal calf serum (unless overwise specified). Cells were cultured at 37 °C in a 5% CO_2 humidified atmosphere.

6.4.2. Cell viability on monolayer cultures (2D)

Briefly, cells were grown in 96-well plates in the presence of increasing concentrations of each compound (from 50 to 0.01 μM) for 48 h. Cell viability was then assessed using the CellTiter 96® AQueous One Solution Cell Proliferation Assay from Promega according to manufacturer's instructions. Each experiment was done in triplicate and IC_{50} were determined from the dose-response curves according to the signal given by the control (0.5% DMSO) set at 100% viability.

6.4.3. Cell viability on spheroid cultures (3D)

U-2 OS cells (5000 cells/well) and HCT116 (1500 cells/well) were seeded in 96-well black ULA plates (Ultra Low Adherence, Corning Incorporated, USA). After centrifugation at 200g for 10 min, spheroids were allowed to form for 3 days in order to reach 400 μm in diameter.

Compounds were then added at 1, 5 and 10 µM. Cell viability was measured after 7 days using the CellTiter-Glo® Luminescent Cell Viability Assay (Promega) following the manufacturer's protocol.

6.4.4. H3T3ph immunofluorescence

HCT116 cells were grown on coverslips, treated for 16 h than fixed with 4% paraformaldehyde in PBS, permeabilized by 0.15% Triton-X100 for 2 minutes, blocked for 15 minutes in 4% BSA in PBS and processed using standard immunofluorescence protocols. The primary antibody was an anti-phospho-Thr3 Histone H3 from Millipore (1/1000 dilution). Coverslips were mounted with Vectashield containing DAPI (Vector Laboratories). Images were acquired with a Coolsnap HQ_2 CCD camera (Photometrics) on a Zeiss Axio microscope (Carl Zeiss) using a 63x NA 1.40 objective. Image acquisition and processing were performed using Metamorph (Molecular Device). Quantification of signal intensity was performed using ImageJ software (NIH).

6.5 Protein crystallography

Recombinant Haspin kinase domain was purified as described previously [28]. Crystallization was perform using the protein at 14 mg/ml mixed with the inhibitor **2a** at 1 mM, and sitting drop vapour diffusion method at 4 °C with the condition containing 60% MPD, 0.1M SPG 6.5. Diffraction data were collected at Swiss Light Source beamline X06DA, and were processed and scaled with XDS [29] and Scala from CCP4 suite [30]. Structure was solved by molecular replacement using Phaser [31] and the published coordinates of haspin [28]. Model rebuilding was performed in COOT [32] and the structure was refined using REFMAC5 [33]. The data collection and refinement statistics are summarized in the table 3 below.

Complex	**Haspin-2a**
PDB codes	7OPS
Data Collection	
Resolution[a] (Å)	45.70-2.38 (2.51-2.38)
Space group	$P\ 2_12_12_1$
Cell dimensions	a=78.1, b=79.1, c=82.3 Å
	α= β=γ=90.0°
Number of unique reflections	20,503 (2,925)
Completeness (%)	99.8 (99.5)
I/σI	9.4 (2.0)
R_{merge} (%)	0.157 (0.884)

CC (1/2)	0.995 (0.708)
Redundancy	6.6 (6.7)
Refinement	
Number atoms in refinement (P/L/O)[b]	2.627/ 19/ 161
B factor (P/L/O)[b] (Å^2)	39/ 39/ 40
R_{fact} (%)	17.7
R_{free} (%)	22.8
rms deviation bond[c] (Å)	0.012
rms deviation angle[c] (°)	1.3
Molprobity Ramachandran	
Favor (%)	98.16
Outlier (%)	0

[a] Value in brackets indicates high-resolution shell statistics.

[b] P/L/O indicates protein, ligand and others.

[c] rms indicates root-mean-square

Table 3. X-ray data collection and refinement statistics of Haspin-Compound **2a** structure

Acknowledgments

The authors thank Aurélie Job for HPLC analysis and Margaux Macaigne for technical assistance on kinase assays. The authors thank La Ligue Contre le Cancer/Comité du Cantal/Comité Grand -Ouest (districts 29, 22, 56, 35, 45 and 79) and ITMO Cancer AVIESAN (National Alliance for Life Sciences & Health) within the framework of the Cancer Plan for financial support (FA, BB, FG, BJ, PM and SR). The Auvergne Region (Jeune Chercheur Program) is also acknowledged for funding (WZ, FA, FG and PM) as well as the French Ministry of Higher Education and Research for YJE and MD PhD fellowships. SK and AC are grateful for support by the SGC, a registered charity (no. 1097737) that receives funds from AbbVie, BayerAG, Boehringer Ingelheim, the Canada Foundation for Innovation, Eshelman Institute for Innovation, Genentech, Genome Canada through Ontario Genomics Institute [OGI-196], EU/EFPIA/OICR/McGill/KTH/Diamond, Innovative Medicines Initiative 2 Joint Undertaking [EUbOPEN grant 875510], Janssen, Merck KGaA, Merck & Co, Pfizer, Takeda and Wellcome. SK is also grateful for support by the German translational cancer network (DKTK) as well as the Frankfurt Cancer Institute (FCI). The authors thank staff at Swiss Light Source for their assistance during diffraction data collection.

References

[1] J. M. G. Higgins. Haspin-like proteins: a new family of evolutionarily conserved putative eukaryotic protein kinases. *Protein Sci*. **2001**, *10*, 1677-1684. https://doi.org/10.1110/ps.49901

[2] J. Eswaran, D. Patnaik, P. Filippakopoulos, F. Wang, R. L. Stein, J. W. Murray, J. M. G. Higgins, S. Knapp. Structure and functional characterization of the atypical human kinase haspin. *Proc. Natl. Acad. Sci. USA* **2007**, *104*, 20523-20528. https://doi.org/10.1073/pnas.0901989106

[3] C. Dominguez-Brauer, K. L. Thu, J. M. Masson, H. Blaser, M. R. Bray, T. W. Mak. Targeting mitosis in cancer: emerging strategies. *Mol. Cell* **2015**, *60*, 524-536. https://doi.org/10.1016/j.molcel.2015.11.006

[4] D. Huertas, M. Soler, J. Moreto, A. Villanueva, A. Martinez, A. Vidal, M. Charlton, D. Moffat, S. Patel, J. McDermott, J. Owen, D. Brotherton, D. Krige, S. Cuthill, M. Esteller. Antitumor activity of a small-molecule inhibitor of the histone kinase haspin. *Oncogene* **2012**, *31*, 1408-1418. https://doi.org/10.1038/onc.2011.335

[5] O. Feizbakhsh, M. Place, X. Fant, F. Buron, S. Routier, S. Ruchaud. The mitotic kinase haspin and its inhibitors. Biochemistry, genetics and molecular biology "Protein phosphorylation". Edited by Claude Prigent 2017, Chap. 2, 31-47. http://dx.doi.org/10.5772/intechopen.70732

[6] A. De Antoni, S. Maffini, S. Knapp, A. Musacchio, S. Santaguida. A small molecule inhibitor of haspin alters the kinetochore functions of aurora B. *J. Cell. Biol*. **2012**, *199*, 269-284. https://doi.org/10.1083/jcb.201205119

[7] D. Patnaik, J. Xian, M. A. Glicksman, G. D. Cuny, R. L. Stein, J. M. G. Higgins. Identification of small molecule inhibitors of the mitotic kinase haspin by high-throughput screening using a homogeneous time-resolved fluorescence resonance energy transfer assay. *J. Biomol. Screen*. **2008**, *13*, 1025-1034. https://doi.org/10.1177/1087057108326081

[8] G. D. Cuny, M. Robin, N. P. Ulyanova, D. Patnaik, V. Pique, G. Casano, J.-F. Liu, X. Lin, J. Xian, M. A. Glicksman, R. L. Stein, J. M. G. Higgins. Structure-activity relationship study of acridine analogs as haspin and Dyrk2 kinase inhibitors. *Bioorg. Med. Chem. Lett*. **2010**, *20*, 3491-3494. https://doi.org/10.1016/j.bmcl.2010.04.150

[9] N. G. Amoussou, A. Bigot, C. Roussakis, J.-P. H. Robert. Haspin: a promising target for the design of inhibitors as potent anticancer drugs. *Drug Discov. Today* **2018**, *23*, 409-415. https://doi.org/10.1016/j.drudis.2017.10.005

[10] G. Manning, D. B. Whyte, R. Martinez, T. Hunter, S. Sudarsanam. The protein kinase complement of the human genome. *Sciences* **2002**, *298*, 1912-1934. https://doi.org/10.1126/science.1075762

[11] K. Rüben, A. Wurzlbauer, A. Walte, W. Sippl, F. Bracher, W. Becker. Selectivity profiling and biological activity of novel beta-carbolines as potent and selective DYRK1 kinase inhibitors. *Plos One* **2015**, *10*: e0132453. https://doi.org/10.1371/journal.pone.0132453

[12] J. Higgins, D. Patnaik, N. Ulyanova, R. L. Stein, J. Xian, M. Glicksman, G. D. Cuny. Beta-carbolines as inhibitors of haspin and dyrk kinases. US20130231360 (2013).

[13] J. Higgins, G. D. Cuny, M. Gliscksman, D. Patnaik, M. Robin, R. L. Stein, J. Xian. Acridines as inhibitors of haspin and dyrk kinases. US20130102627 (2013).

[14] M. Schröder, A. N. Bullock, O. Fedorov, F. Bracher, A. Chaikuad, S. Knapp. DFG-1 residue controls inhibitor binding mode and affinity, providing a basis for rational design of kinase inhibitor selectivity. *J. Med. Chem*. **2020**, *63*, 10224-10234. https://doi.org/10.1021/acs.jmedchem.0c00898

[15] V. Němec, M. Hylsová, L. Maier, J. Flegel, S. Sievers, S. Ziegler, M. Schröder, B.-T. Berger, A. Chaikuad, B. Valčíková, S. Uldrijan, S. Drápela, K. Souček, H. Waldmann, S. Knapp, K. Paruch. Furo[3,2-*b*]pyridine: a privileged scaffold for highly selective kinase inhibitors and effective modulators of the hedgehog pathway. *Angew. Chem. Int. Ed*. **2019**, *58*, 1062-1066. https://doi.org/10.1002/anie.201810312

[16] Y. J. Esvan, W. Zeinyeh, T. Boibessot, L. Nauton, V. Théry, S. Knapp, A. Chaikuad, N. Loaëc, L. Meijer, F. Anizon, F. Giraud, P. Moreau. Discovery of pyrido[3,4-g]quinazoline derivatives as CMGC family protein kinase inhibitors: design, synthesis, inhibitory potency and X-ray co-crystal structure. *Eur. J. Med. Chem*. **2016**, *118*, 170-177. https://doi.org/10.1016/j.ejmech.2016.04.004

[17] W. Zeinyeh, Y. J. Esvan, L. Nauton, N. Loaëc, L. Meijer, V. Théry, F. Anizon, F. Giraud, P. Moreau. Synthesis and preliminary in vitro kinase inhibition evaluation of new diversely substituted pyrido[3,4-*g*]quinazoline derivatives. *Bioorg. Med. Chem. Lett*. **2016**, *26*, 4327-4329. https://doi.org/10.1016/j.bmcl.2016.07.032

[18] H. Tazarki, W. Zeinyeh, Y. J. Esvan, S. Knapp, D. Chatterjee, M. Schröder, A. C. Joerger, J. Khiari, B. Josselin, B. Baratte, S. Bach, S. Ruchaud, F. Anizon, F. Giraud, P. Moreau. New pyrido[3,4-*g*]quinazoline derivatives as CLK1 and DYRK1A inhibitors: synthesis, biological evaluation and binding mode analysis. *Eur. J. Med. Chem.* **2019**, *166*, 304-317. https://doi.org/10.1016/j.ejmech.2019.01.052

[19] W. Zeinyeh, Y. J. Esvan, B. Josselin, B. Baratte, S. Bach, L. Nauton, V. Théry, S. Ruchaud, F. Anizon, F. Giraud, P. Moreau. Kinase inhibitions in pyrido[4,3-*h*] and [3,4-*g*]quinazolines: synthesis, SAR and molecular modeling studies. *Bioorg. Med. Chem*. **2019**, *27*, 2083-2089. https://doi.org/10.1016/j.bmc.2019.04.005

[20] Y. J. Esvan, B. Josselin, B. Baratte, S. Bach, S. Ruchaud, F. Anizon, F. Giraud, P. Moreau. Synthesis and kinase inhibitory potencies of new pyrido[3,4-*g*]quinazolines substituted at the 8-position. *Arkivoc* **2020**, *7*, 105-116. https://doi.org/10.24820/ark.5550190.p011.268

[21] S. Guihéneuf, L. Paquin, F. Carreaux, E. Durieu, L. Meijer, J. P. Bazureau. An efficient approach to dispacamide A and its derivatives. *Org. Biomol. Chem.* **2012**, *10*, 978-987. https://doi.org/10.1039/C1OB06161E

[22] C. M. Timmers, W. F. J. Karstens. Bicyclic heteroaromatic compounds. WO2002024703.

[23] M. E. Salvati, R. M. Attar, M. M. Gottardis, J. A. Balog, D. A. Pickering, R. L. Martinez, C. Sun. Fused cyclic succinimide compounds and analogs thereof, modulators of nuclear hormone receptor function. WO2002067939.

[24] V. Fagan, S. Bonham, M. P. Carty, P. Saenz-Méndez, L. A. Eriksson, F. Aldabbagh. Compare analysis of the toxicity of an iminoquinone derivative of the imidazo[5,4-*f*]benzimidazoles with NAD(P)H:quinones as NQ01 substrates. *Bioorg. Med. Chem*. **2012**, *20*, 3223-3232. https://doi.org/10.1016/j.bmc.2012.03.063

[25] J. Elie, O. Feizbakhsh, N. Desban, B. Josselin, B. Baratte, A. Bescond, J. Duez, X. Fant, S. Bach, D. Marie, M. Place, S. B. Salah, A. Chartier, S. Berteina-Raboin, A. Chaikuad, S. Knapp, F. Carles, P. Bonnet, F. Buron, S. Routier, S. Ruchaud. Design of new disubstituted imidazo[1,2-*b*]pyridazine derivatives as selective Haspin inhibitors. Synthesis, binding mode and anticancer biological evaluation. *J. Enzyme Inhib. Med. Chem*. **2020**, *35*, 1840-1853. https://doi.org/10.1080/14756366.2020.1825408

[26] E. F. Pettersen, T. D. Goddard, C. C. Huang, G. S. Couch, D. M. Greenblatt, E. C. Meng, T. E. Ferrin. UCSF Chimera-A visualization system for exploratory research and analysis. *J. Comput. Chem.* **2004**, *13*, 1605-1612. https://doi.org/10.1002/jcc.20084

[27] H. Zegzouti, M. Zdanovskaia, K. Hsiao, S. A. Goueli. ADP-Glo: A bioluminescent and homogeneous ADP monitoring assay for kinases. *Assay Drug Dev. Technol*. **2009**, *7*, 560-572. https://doi.org/10.1089/adt.2009.0222

[28] C. Heroven, V. Georgi, G. K. Ganotra, P. Brennan, F. Wolfreys, R. C. Wade, A. E. Fernández-Montalván, A. Chaikuad, S. Knapp. Halogen-aromatic π interactions modulate inhibitor residence times. *Angew. Chem. Int. Ed*. **2018**, *57*, 7220-7224. https://doi.org/10.1002/anie.201801666

[29] W. Kabsch. XDS. *Acta Cryst. D* **2010**, *66*, 125-132. https://doi.org/10.1107/S0907444909047337

[30] L. Potterton, J. Agirre, C. Ballard, K. Cowtan, E. Dodson, P. R. Evans, H. T. Jenkins, R. Keegan, E. Krissinel, K. Stevenson, A. Lebedev, S. J. McNicholas, R. A. Nicholls, M. Noble, N. S. Pannu, C. Roth, G. Sheldrick, P. Skubak, J. Turkenburg, V. Uski, F. von Delft, D. Waterman, K. Wilson, M. Winn, M. Wojdyr. CCP4i2: the new graphical user interface to the CCP4 program suite. *Acta Cryst. D* **2018**, *74*, 68-84. https://doi.org/10.1107/s2059798317016035

[31] A. J. McCoy, R. W. Grosse-Kunstleve, P. D. Adams, M. D. Winn, L. C. Storoni, R. J. Read. Phaser crystallographic software. *J. Appl. Crystallogr*. **2007**, *40*, 658-674. https://doi.org/10.1107/s0021889807021206

[32] P. Emsley, B. Lohkamp, W. G. Scott, K. Cowtan. Features and development of Coot. *Acta Cryst. D* **2010**, *66*, 486-501. https://doi.org/10.1107/s0907444910007493

[33] G. N. Murshudov, P. Skubák, A. A. Ledebev, N. S. Pannu, R. A. Steiner, R. A. Nicholls, M. D. Winn, F. Long, A. A. Vagin. REFMAC5 for the refinement of macromolecular crystal structures. *Acta Cryst. D* **2011**, *67*, 355-367. https://doi.org/10.1107/S0907444911001314